P.-Q. Elias
(ONERA)

E-mail: Paul-Quentin.Elias@onera.fr

DOI : 10.12762/2015.AL10-03

Numerical Simulations on the Effect and Efficiency of Long Linear Energy Deposition Ahead of a Supersonic Blunt Body: Toward a Laser Spike

The effect of single or repetitive linear energy depositions in front of a supersonic blunt body is computed using the CEDRE flow solver. The CFD Code models the effect of a laser-induced energy deposition, as obtained for example using the long filaments created by a femtosecond laser. Single energy depositions show that significant transient drag reductions are obtained, due to the interaction of the heated core, created by the energy release, with the bow shock. When the deposition is repeated, cumulative effects are important and quasi-steady or unsteady flow regimes are obtained, depending on the power and repetition frequency. This behavior is similar to that obtained with supersonic spiked blunt bodies, acting like a laser spike. This system can lead to 15%-20% fuel savings, depending on the energy deposition efficiency.

Introduction

There has been a substantial amount of experimental and theoretical work devoted to the use of plasma-based devices for flow control [1]–[4]. Plasmas mainly act on the flow through two channels: gas heating and volume force in the region where the plasma is not quasi-neutral or where a magnetic field exists. The location of the forcing action of the plasma depends on its generation mechanism. There are two main ways of creating the plasma. First, it can be generated by electrodes exposed to the flow, or partly exposed (with dielectric barriers). In this case, the generated plasma is most of the time confined in the vicinity of the body; this means that the forcing is close to the body surface. Second, the plasma can be generated with an intense electromagnetic radiation focused in the flow. When the radiation is intense enough, gas breakdown occurs and a plasma is generated. In this case, the generation can be near a surface, but also in the volume of the flow and, more interestingly, possibly upstream of the body. This plasma couples with the incoming radiation and heats up, enabling the deposition of energy in the flow ahead of the body.

This possibility has led several authors to study the use of laser-induced or microwave-induced energy deposition upstream of a supersonic body for flow control. For example, it was shown experimentally that laser-induced plasma created upstream of a supersonic body could trigger the transition from a regular to a Mach reflection, or temporarily decrease the wall heat flux in an Edney type IV shock interaction [5] [6]. The use of laser energy deposition has also been considered to reduce the supersonic drag of blunt bodies. Indeed, it is known that supersonic blunt bodies can have their wave drag significantly decreased when using mechanical spike or counter-flowing jets. Using repetitively pulsed laser sources, several authors have shown the possibility of decreasing the drag of blunt bodies with repetitive point energy deposition [7] [8]. For example, Sakai et al have studied the effect of pulsed laser energy deposition upstream of a blunt body. They have shown numerically and experimentally that there is a 25% drag reduction, for a repetition frequency of f=60 kHz, in front of a cylinder at M=2 [9] [10].

These works have demonstrated the ability of pulsed repetitive point energy deposition to significantly reduce the drag. However, a key point for this reduction to be applicable is the overall efficiency. This efficiency quantifies the fuel savings taking into account the whole drag reduction system, with the energy conversion efficiencies of the various sub-systems. These sub-systems include the power generator, the laser and the energy coupling of the plasma. In order to assess the efficiency of the energy deposition, some authors [11] use the aerodynamic efficiency η_{ae}, defined as:

$$\eta_{ae} = \frac{U_\infty \Delta D}{fE} \quad (1)$$

Where U_∞ is the upstream velocity of the flow, ΔD is the drag reduction (in Newtons), f is the repetition frequency of the laser and E is the laser energy per pulse. Due to the fact that the efficiencies of the

laser and the energy conversion from the engine can be quite low, the value of η_{ae} needs to be as high as possible to ensure that the cost of the drag reduction system does not outweigh its benefit.

A strategy to increase this efficiency is to try to change the shape of the energy deposition. Indeed, point energy deposition requires a high repetition frequency to reach a steady state. If the deposition were elongated, lower repetition frequencies might be needed and η_{ae} would increase. This idea is guided by the recent progress of femtosecond lasers, which are known to create thin ionized channels [12] [13]. These channels can be used to guide an electric discharge and there is currently an ongoing research effort to couple energy to this ionized channel using various mechanisms: more powerful nanosecond lasers [15], pulsed discharges or microwave excitation [16].

This prospect of laser-assisted linear energy deposition has led several authors to numerically address their use for drag reduction. Kremeyer et al have modeled linear energy depositions on the axis of supersonic cones and have shown that efficiencies between 5 and 65 can be obtained, depending on the Mach number and the shape of the energy deposition [17]. As a rule, the higher the Mach number is, the larger η_{ae} is. Sutton has analytically examined the effect of cylindrical blast waves generated upstream of fast-burning rockets and has shown that for large enough Mach numbers, long pulses can lead to fuel savings [18].

The previous studies have shown that an efficient drag reduction is feasible using a linear energy deposition upstream of the body. However, these studies focused on a single pulse event and therefore have to extrapolate to conclude on the steady state operation of the system. Reaching a steady state is important, in particular when analyzing the cumulative effect of repetitive energy deposition. In addition, another important point to assess the efficiency of the whole system is linked to the heating processes in the plasma. Indeed, only a fraction of the deposited energy is effectively used to produce the blast wave and the hot gas kernel. This fraction is driven by various loss processes in the plasma. Therefore, as in the above-mentioned works, the perfect gas assumption might overestimate the efficiency of the laser-induced drag reduction.

As a consequence, this paper focuses on the modeling of long linear energy deposition in front of a supersonic blunt body and on the corresponding numerical simulations. The two limitations discussed above are specifically addressed, first by considering a self-consistent modeling of the repetitive energy addition and, second, by using real gas properties for the flow. In order to gain insight on the applicability of the laser line energy deposition, the test model considered will have dimensions and flight conditions consistent with what can be achieved in a supersonic wind tunnel.

Virtual Spike modeling

Local Thermodynamic Equilibrium hypothesis

The modeling of the heat deposition by the laser requires the way in which the input laser energy is transferred to the gas to be considered. It will be assumed here that the energy is supplied by a filamenting femtosecond laser, combined with a secondary energy source (such as a combined nanosecond laser, or a micro-wave source).

The main energy transfers between the energy modes of the gas are shown in Figure 1. In a simplistic form, the energy transfers are as follows. During the laser breakdown and subsequent plasma heating, the power is transferred to the electrons, whose temperature increases. This rise in temperature leads to inelastic collisions, creating excited, dissociated or ionized molecules. The heavier species in the plasma are then mainly heated by inelastic collisions with the excited species. This increase in internal energy induces pressure gradients that lead to a macroscopic transfer of mass and momentum in the fluid and builds up macroscopic kinetic energy. In principle, a self-consistent modeling of a laser-induced energy deposition should take into account the breakdown phase and the following additional energy input; the various loss terms should be accounted for, such as the plasma chemistry, the radiative losses, the diffusion losses, etc. [19][20][21][22]. This approach is beyond the scope of this study. In previous works, the incoming flow was assumed to behave as a perfect gas. In this situation, the transfer between the potential energy and the microscopic kinetic energy modes is frozen. All of the energy input is used to increase the temperature. Consequently, in order to avoid unphysical temperatures, only a fraction of the energy is used [8]. This fraction is poorly known: it depends strongly on the plasma processes during the breakdown and the energy deposition.

On the contrary, another solution is to assume that the transfers between the energy modes (potential and microscopic) are so fast that the plasma created by the laser reaches thermodynamic equilibrium. In this case, the input energy is spread over all of the energy modes. This hypothesis is interesting because it gives the lower bound for the plasma temperature. Being a kind of worst case scenario, it is useful to address the question of the efficiency of the laser-induced drag reduction. It also enables a simpler modeling, since only a single fluid modeling of the plasma is needed.

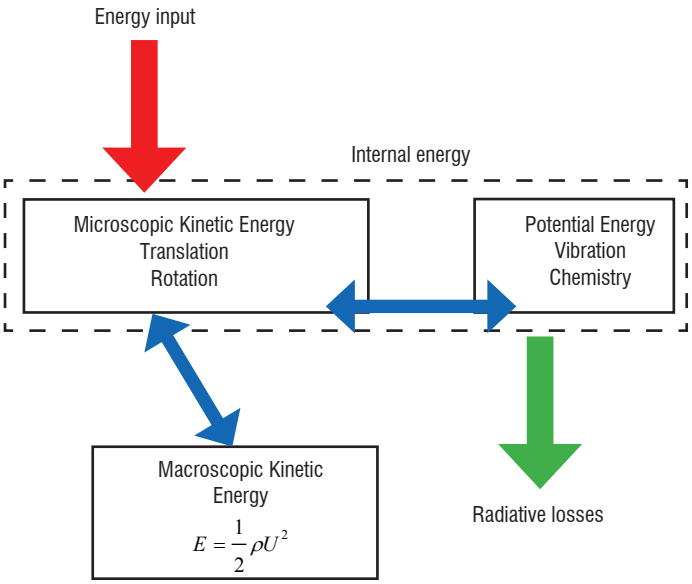

Figure 1 - Energy modes (rectangles) and energy transfers (arrows) in a gas with an external heating source Air properties

Air properties

The properties of air at local thermodynamic equilibrium are obtained from [23]. This tabulation gives these properties for a temperature up to 50,000 K and for a wide pressure range. For the purpose of our analysis, the following properties are needed: the gas molar enthalpy $h(T,p)$ and molar entropy $s(T,p)$, its heat capacity at constant pressure $c_p(T,p)$ and its molar mass $M(T,p)$. Note that the molar mass decreases at higher temperatures, because of the dissociation of N_2 and O_2. Finally,

the transport coefficients are also needed (viscosity, conductivity). As an example, in Figure 2, the heat capacity and the thermal conductivity of air at local thermodynamic equilibrium (*LTE*) are given. The heat capacity shows several peaks that correspond to the dissociation of the diatomic molecules in the mixture.

Modeling of the power deposition

The laser energy deposition is modeled through a source term σ in the energy equation. Assuming that the flow is described by the Navier-Stokes equations, using temperature and pressure dependent thermophysical coefficients:

$$\begin{aligned}
&\frac{\partial \rho}{\partial t}+\nabla(\rho \boldsymbol{u})=0 \\
&\frac{\partial \rho \boldsymbol{u}}{\partial t}+\nabla(\rho \boldsymbol{u}\boldsymbol{u})=-\nabla p+\nabla \overline{\overline{\tau}} \\
&\frac{\partial \rho\left(e+\frac{1}{2}u^2\right)}{\partial t}+\nabla\left(\rho \boldsymbol{u}\left(e+\frac{1}{2}u^2\right)\right)=-\nabla \mathbf{q}+\nabla\left(\overline{\overline{\tau}}\boldsymbol{u}\right) \\
&\qquad -\nabla(p\boldsymbol{u})+\boldsymbol{\sigma}
\end{aligned} \tag{2}$$

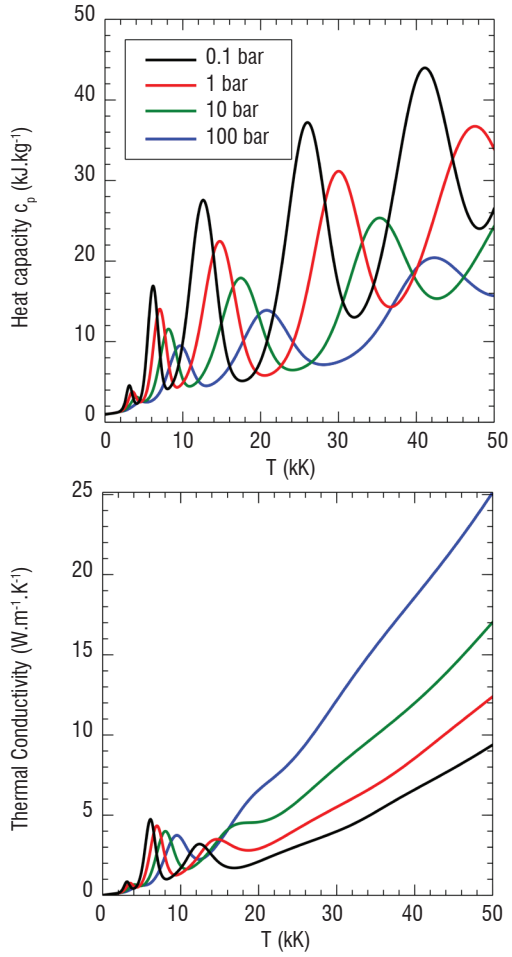

Figure 2 - Heat capacity and thermal conductivity of *LTE* air, for different pressures

The source term can be described as a time and space dependent function:

$$\sigma(r,z,t)=Ef(r,z)g(t) \tag{3}$$

Where E is the total pulse energy, and f and g are the space and time modulation. In this study, the energy is deposited during a period of length T, in a cylinder of radius r and length L

$$g(t)=\begin{cases}\dfrac{1}{T} \text{ if } t\in[0,T] \\ 0 \text{ otherwise}\end{cases} \tag{4}$$

$$f(y,z)=\begin{cases}\dfrac{1}{\pi r^2 L} \text{ if } y\in[0,r] \text{ and } z\in[-L+z_0,z_0] \\ 0 \text{ otherwise}\end{cases} \tag{5}$$

During the energy deposition phase, inside the cylinder, the volumetric power source is $\sigma=\dfrac{E}{T}\dfrac{1}{\pi r^2 L}$.

Numerical methods

The computations in this study are performed with the CEDRE CFD code, developed at Onera [24]–[26]. The code is a multiphysics tool, including the CHARME module, a finite volume gas dynamics solver on polyhedral meshes.

The following methodology is used for this study. First, the steady-state reference flow without energy deposition is sought, using a local time step. Once the code converges to the steady solution, the heat deposition is activated and the flow time evolution is tracked using an implicit two-step Runge Kutta algorithm. For each step, a 2nd order space discretization is used; the convective part of the fluxes is computed using the Van Leer method.

The computations are performed on axisymmetric meshes, taking into account the axial symmetry of the problem. Unstructured meshes are used. They are refined close to the body, using structured patches for the boundary layer discretization. The distance to the body wall of the first cell is 4-5 μm. Assuming that the flow conditions behind the bow shock are those obtained behind a plane shock, the viscous distance y^+ of the first cell is y^+=1.2-1.5. Similarly, the region close to the body axis is refined with structured patches. In the region of the energy deposition, the cell width is 45 μm, while their length is 200 μm The base mesh has 10^5 cells.

Results

This section presents the results of the computation. First, the test configuration and the reference flow is described. Then the effect of a single laser energy deposition is discussed, including a parametric study on the effect of the deposition duration and length. Finally, the effect of repetitive pulses is discussed.

Test model configuration and reference flow

A schematic diagram of the test model used for the study is shown in Figure 3. The test model is a standard HB-1 model [27]. The freestream conditions, as given in Table 1, reproduce typical wind-tunnel conditions achievable in the ONERA R1Ch wind tunnel.

The laser energy deposition is activated for a period T, in a cylinder of radius R and length L. The cylinder can be located upstream of the bow shock ($dx>0$), or it can start at the stagnation point ($dx=0$).

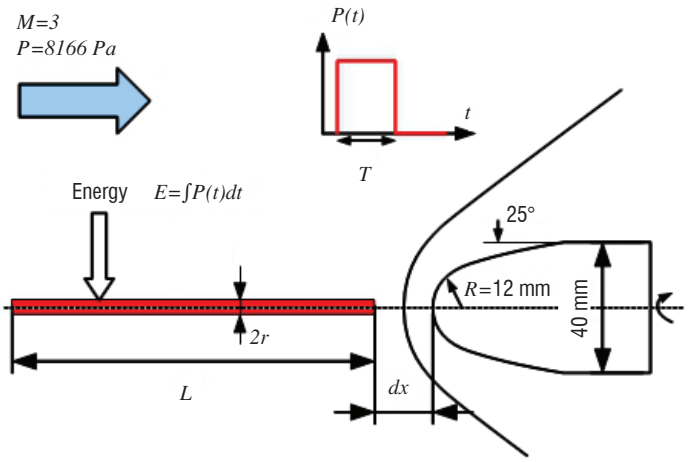

Figure 3 - Shape of the test model and location of the laser energy deposition

The parameters that control the heat deposition are the length of the filament L, its radius r, the filament standoff distance dx, the total energy released E and the duration of the deposition T.

Freestream velocity U_0	652.3 m/s
Freestream temperature T_0	118 K
Freestream pressure p_0	8166 Pa
Unit Reynolds number Re_u	$1.9\times10^7\ m^{-1}$
Mach number M	3

Table 1 - Flow freestream conditions

Although the unit Reynolds number is above $10^7\ m^{-1}$, the computation is performed assuming a laminar flow under the conditions given in Table 1. This is a simplifying assumption of this study, mainly motivated by the fact that the turbulent properties of the high temperature LTE air formed in the heated filament are difficult to model a priori. URANS models, for example, require the knowledge of turbulent coefficients suitable for the chosen turbulence model. These coefficients are quite difficult to assess for the recombining high-temperature plasma considered here. On the other hand, it is important to keep the viscous contribution, since the heated filament interaction will induce large recirculating zone, for which viscous effects are important, even though the flow is assumed to be non-turbulent.

The reference flow is shown in Figure 4. The validity of the converged solution is checked by computing the drag coefficient C^0_x and the shock standoff distance. The drag coefficient and standoff distance are compared to experimental results [28] and a correlation, as given in [29]:

$$\frac{\delta}{R} = 0.143 \exp\left(\frac{3.24}{M_0^2}\right) \tag{6}$$

Case	Drag coefficient C^0_x	Standoff distance δ (mm)
Experiment	0.70 ±0.02	2.46 (Eq. (5))
Base mesh	0.681	2.59
Refined mesh	0.676	2.64

Table 2 – Drag coefficient and standoff distance comparison

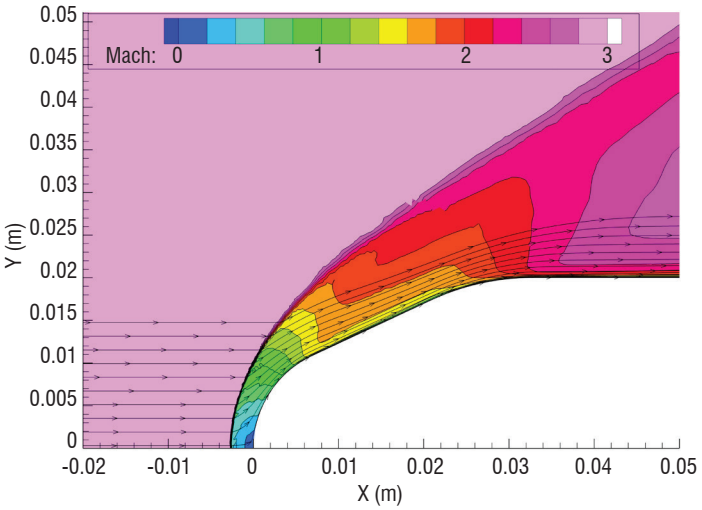

Figure 4 - Steady state flow, Mach number isocontours

Table 2 shows that the computed values for the drag coefficient are within 5% of the measured value. This computed drag falls within the experimental uncertainty of the drag measurement. The 5% discrepancy can be explained as follows: the simulations assume a laminar flow, whereas the experimental reference flow most likely transitions to the turbulent state. Hence, the friction drag is probably underestimated in the computation. The computed standoff distances are within 7% of the standoff obtained from the experimental correlation. Note that the finer mesh (cell dimension divided by two, 4.10^5 cells) does not yield significantly different results (0.8% change in the drag coefficient, 1.9% change in the standoff distance compared to the base mesh), suggesting that mesh convergence is obtained with the base mesh. In the following, the computations will be performed using the base mesh only.

Effect of a single pulse

An overview of the effect of a single pulse is detailed here, considering the following parameters for the energy deposition (Table 3)

Energy E	400 mJ
Deposition duration T	100 ns
Cylinder length L	8R (96 mm)
Cylinder radius r	0.4 mm
Standoff distance dx	0 mm

Table 3 - Energy deposition parameters

For the analysis of a single pulse deposition, the time evolution of the drag shown in Figure 5, Figure 6 and Figure 7 and the pressure isocontours shown in Figure 8 and Figure 9 are considered.

During the deposition stage, the motion of the gas can be neglected, because the convective timescale is much larger than the deposition duration $T \ll r/c_0$ (where c_0 is the speed of sound). The equations (2) can be simplified as:

$$\rho = \rho_o, \qquad \rho_0 \frac{\partial e}{\partial t} = \sigma \tag{7}$$

This means that the gas density remains constant, while the internal energy increases. The energy release induces an increase in the gas pressure at the location of the deposition, while the density remains

nearly constant. This phenomenon creates a baroclinic torque at the location of the shock front, near the symmetry axis. Indeed, the energy release gives rise to a mostly radial pressure gradient, while the density gradient across the shock is axial. The misalignment of the pressure and density profile produces vorticity at the shock front location, such as $(\partial u_z/\partial r) - (\partial u_r/\partial z) < 0$. Since $u_r \approx 0$ close to the axis, this leads to $(\partial u_z/\partial r) < 0$. The flow velocity tends to decrease close to the axis. Additionally, given that the speed of sound in the heated core produced by the energy release is increased significantly, the flow becomes subsonic. This leads to the formation of a large recirculating zone ($t = 50\ \mu$s), where the high pressure gas behind the shock flows upstream like a jet, following the heated core path, in a fashion similar to what is observed with the injection of a counterflowing jet in front of a blunt body [30]. Correlatively, the stagnation pressure decreases. The upstream propagation of the flow corresponds to Phase I in Figure 5, during which the drag decreases nearly linearly. Phase II starts when the counterflowing recirculating bubble reaches the upstream side of the heated core, at $t = 150\ \mu$s. The upstream propagation of the jet ceases and a strong shock appears at its upstream side. During Phase III, the recirculating bubble is pushed downstream by the incoming flow. The bubble now has a toroidal shape, with a heated low pressure core. The drag drop off observed during Phase III, at $t = 375\ \mu$s, is due to the low-pressure core of the vortex impinging on the body wall. This behavior is similar to that observed in [31] with an Euler computation. As the vortex passes along the body, the detached shock reforms in front of the body.

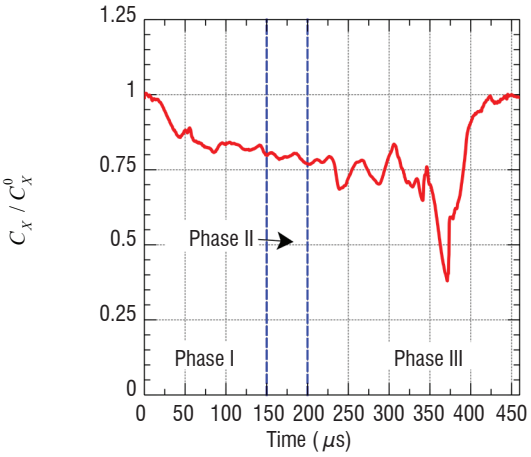

Figure 5 - Time evolution of the reduced drag coefficient. The energy deposition starts at t=0. The value for C^0_X is given in Table 2 (base mesh)

Parametric study

A parametric study is performed by varying the parameters of the energy deposition. The drag evolution is not sensitive to the radius of the deposition (within the range 100-400 μm) and the duration of the deposition (within the range 100-1600 ns), as shown in Figure 6. However, it is significantly modified by the total energy input and the deposition length, as shown in Figure 7. For a constant length L, the cases for 25, 100 and 400 mJ are qualitatively similar. The higher the energy is, the longer Phase II will be, corresponding to the saturation of the counterflowing jet. The case for E=6.25 mJ is qualitatively different, because the toroidal vortex formed is small and the pressure drop at its core is insufficient to induce a large decrease in the drag. For a constant energy E and a varying length, the behavior of the drag is qualitatively the same, although the characteristic times are different. The duration of the interaction does not scale with the deposition length L. It appears that the duration of the interaction is mainly driven by the dynamics of the recirculating bubble.

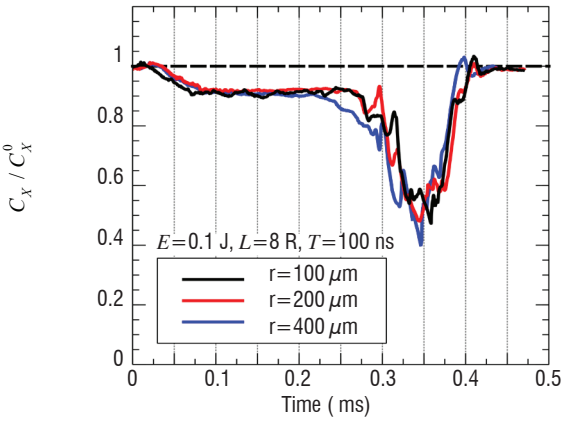

a) Effect of the deposition radius

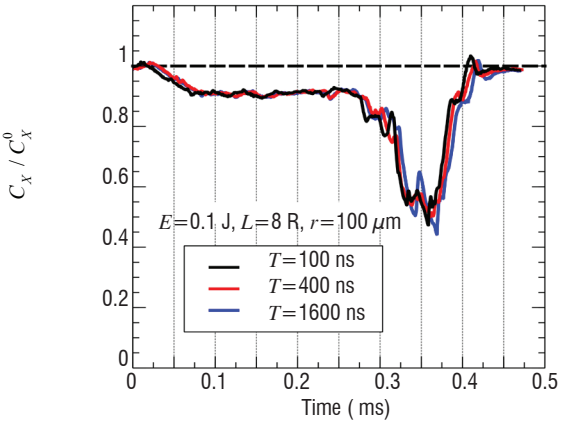

b) Effect of the deposition duration

Figure 6 - Parametric study of the drag evolution: effect of the deposition radius and duration

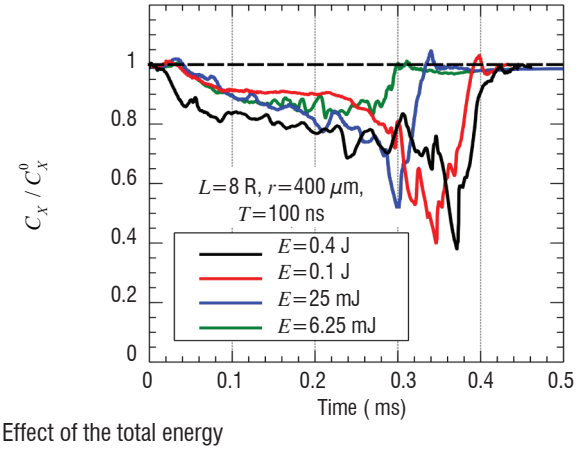

a) Effect of the total energy

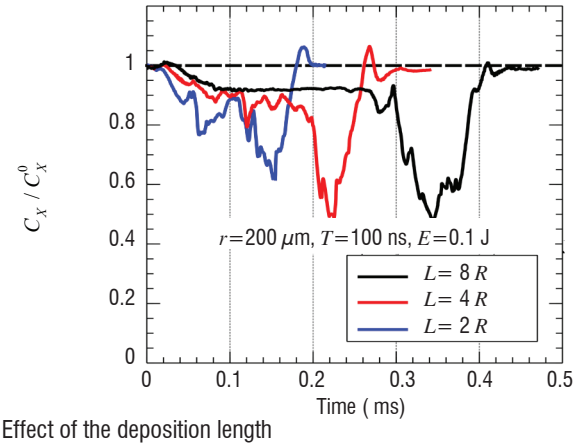

b) Effect of the deposition length

Figure 7 - Parametric study of the drag evolution

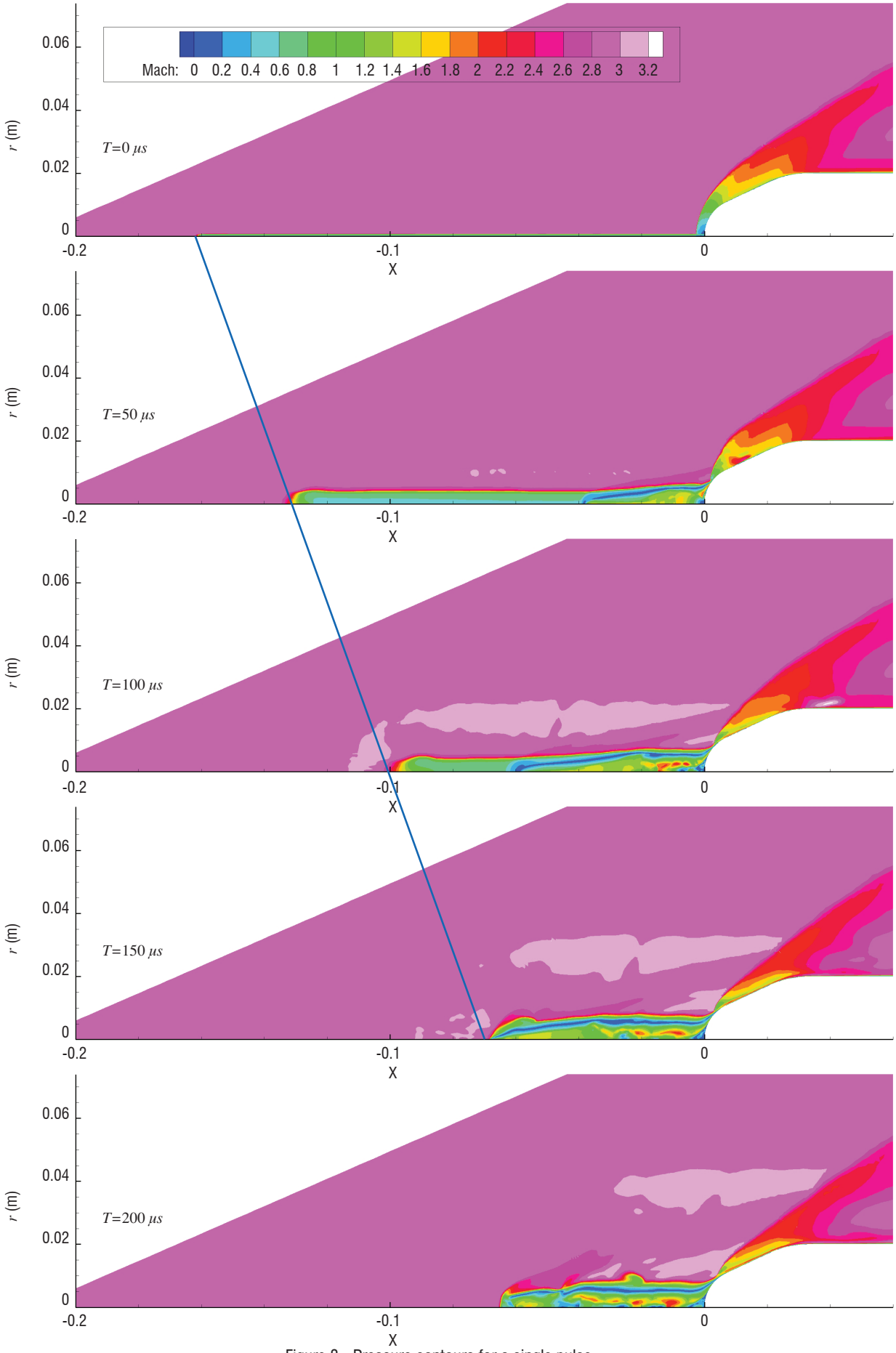

Figure 8 - Pressure contours for a single pulse

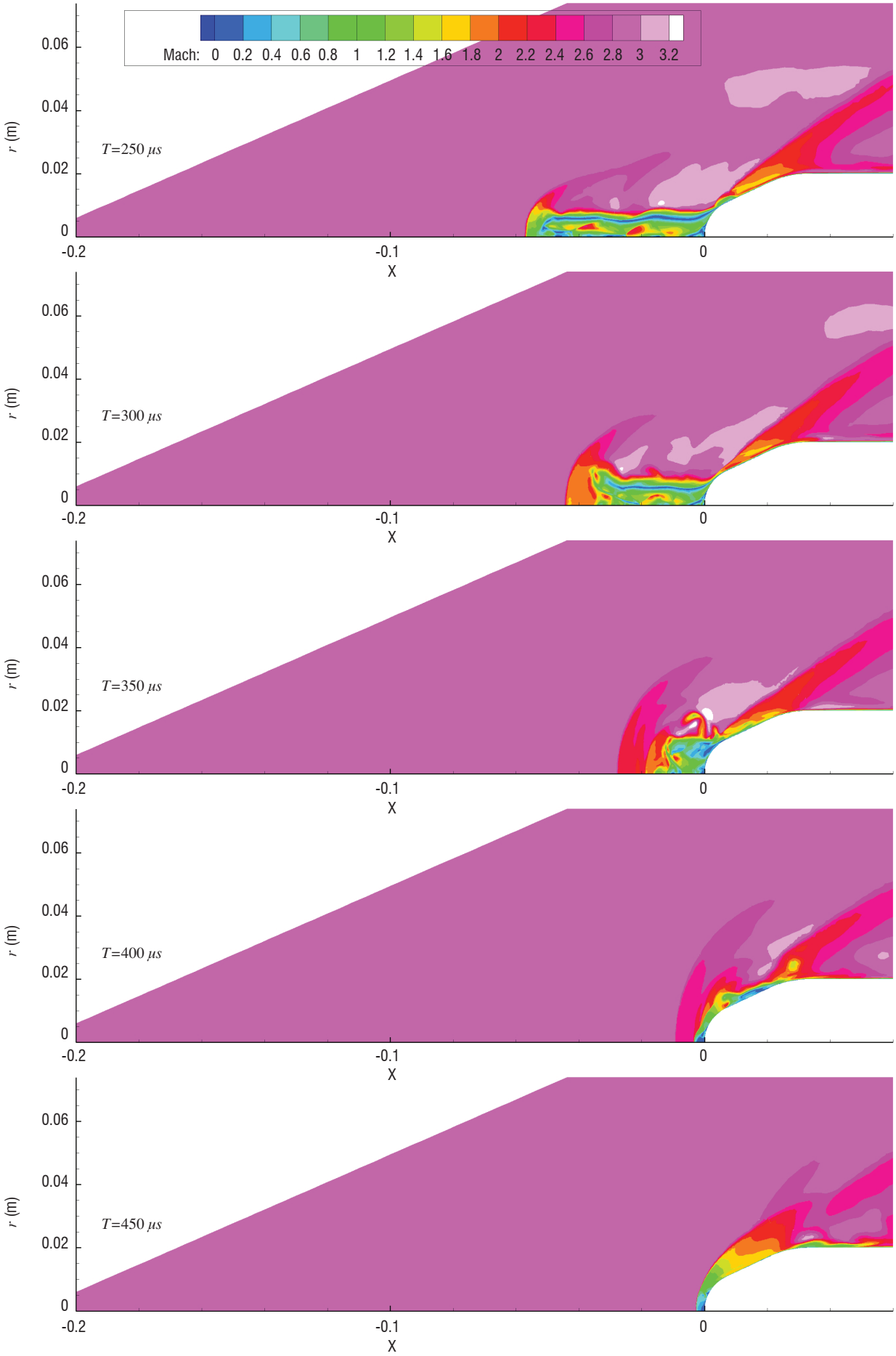

Figure 9 - Pressure contours for a single pulse

Effect of multiple pulses

When examining the effect of repetitive pulsed energy deposition, the above discussion shows that two regimes can be distinguished. In the first regime, the period of the deposition τ is longer or equal to the duration of the filament interaction, as it appears in the time evolution of the drag coefficient. In that case, the mean drag reduction is given by:

$$\langle \Delta \rangle = \frac{1}{\tau}\int_0^{\tau}\left(1-\frac{C_X(t)}{C_X^0}\right)dt \qquad (8)$$

The single pulse cases computed previously are sufficient to assess this regime. In the second regime, τ is shorter than the interaction duration. In this case, it is necessary to take into account the cumulative effect of the repeated energy deposition. The table below summarizes the cases studied for this regime.

Case	Pulse Energy E(mJ)	Pulse Period $\tau(ms)$	Mean Power E/$\tau(W)$
1	6.25	0.1	62.5
2	6.25	0.05	125
3	6.25	0.025	250
4	25	0.2	125
5	25	0.025	1000
6	100	0.1	1000
Continuous	X	X	125

Table 4 –Computational cases for repetitive energy deposition. The deposition duration is 100 ns.

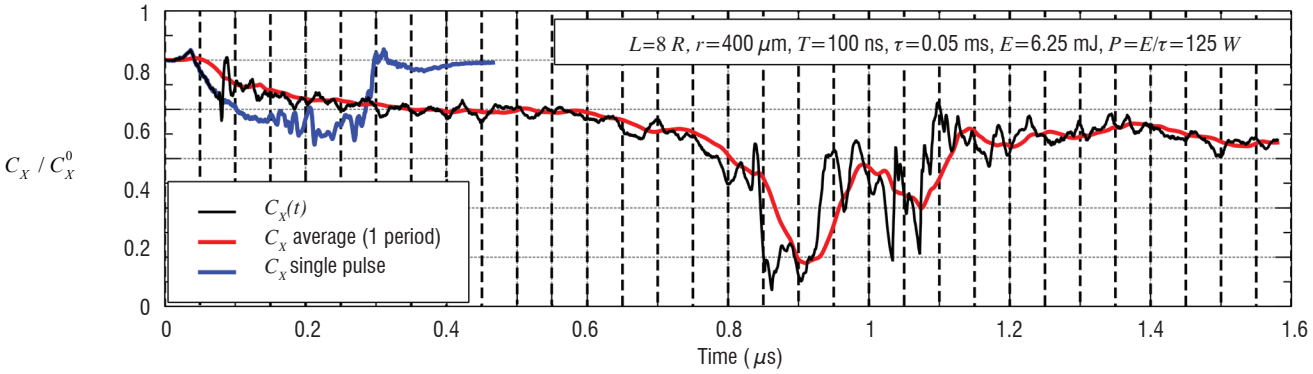

Figure 10 - Case 2, Time evolution of the drag. The dashed line marks the energy deposition time.

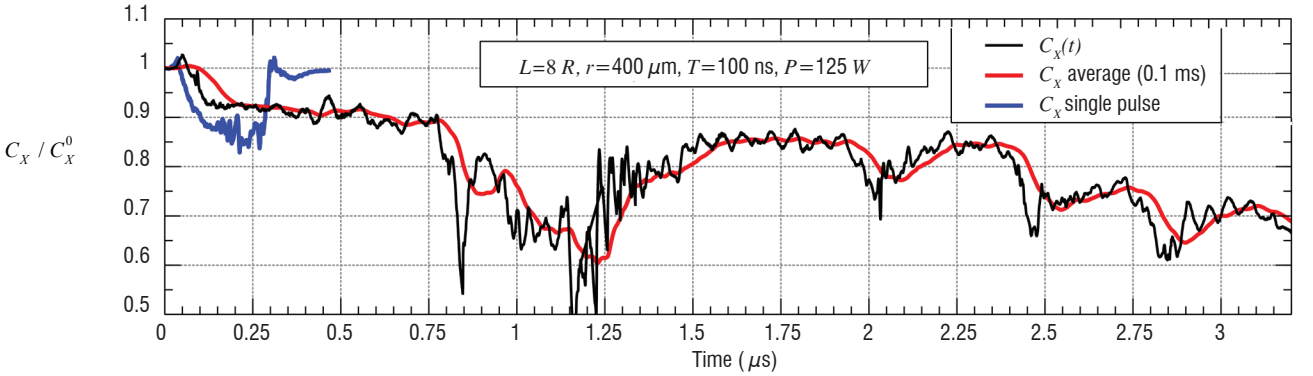

Figure 11 - Continuous deposition, Time evolution of the drag.

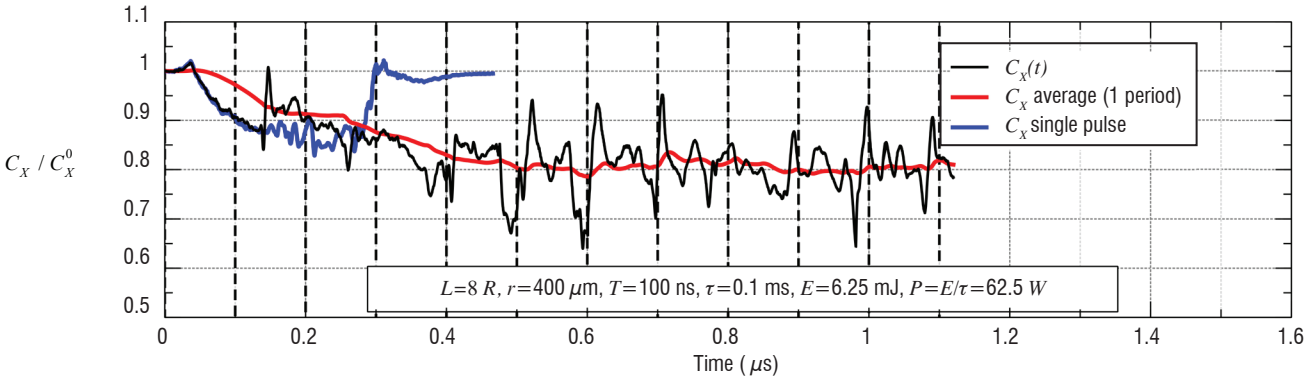

Figure 12 - Case 1, Time evolution of the drag. The dashed line marks the energy deposition time.

For each case, the computation is extended for more than 10 periods, covering at least 1 ms. A first analysis of the results shows that the flow exhibits two behaviors. The first behavior, exemplified in Figure 10, shows a pulsating flow with no stabilization. The drag shows large drop offs, with a seemingly chaotic evolution. This unsteady behavior is also observed in the case of a continuous energy deposition, as shown in Figure 11. In its second behavior, visible in Figure 12, the flow stabilizes and the mean drag reaches a nearly steady value.

Of all of the cases tested in Table 4, Cases 1 and 2 show a stabilization of the drag coefficient, correlated with the formation of a nearly steady recirculating bubble, as shown in Figure 13. The other cases do not reach a quasi-steady state in the time span of the computation. They exhibit a large recirculating bubble, as shown in Figure 14, which collapses repetitively, leading to large fluctuations of the drag coefficient. This situation is similar to what is observed for spiked blunt bodies [32] [33] [34], where pulsating regimes or steady regimes exist, depending of the reduced spike length L/D and also its shape.

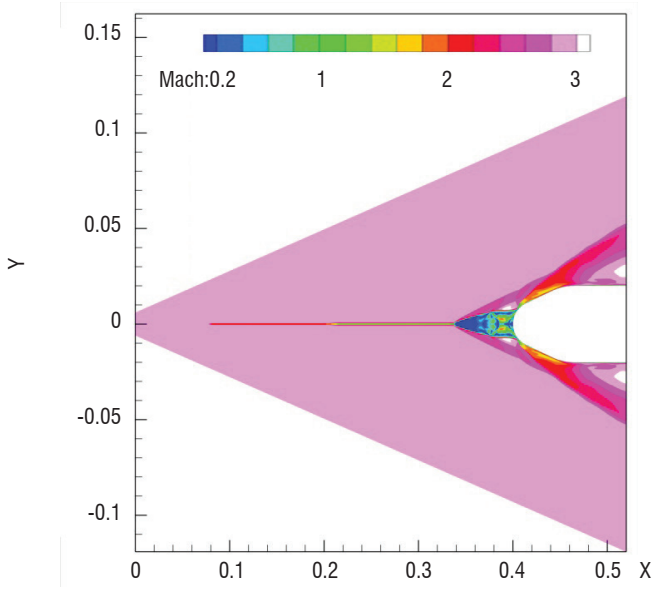

(a) Case 1 : E=6.25 mJ, τ=0.1 ms, P=62.5W, t =1.1 ms

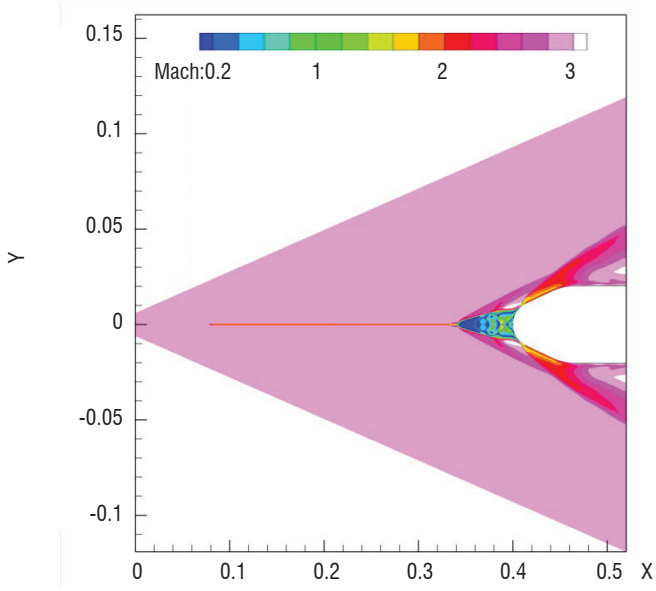

(b) Case 4 : E=25 mJ, τ=0.2 ms, P=125W, t=2.2 ms

Figure 13 - Mach number, Cases 1 and 4. A nearly steady recirculating bubble extends upstream over a diameter of approximately 0.8.

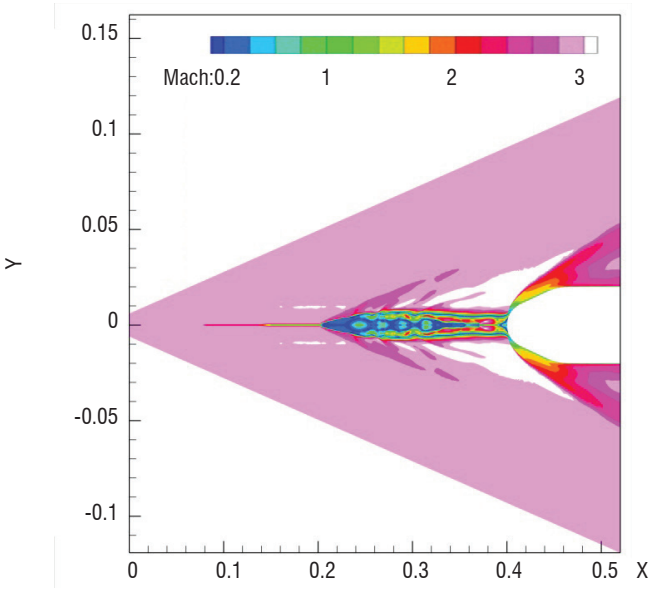

Figure 14 - Mach number, Case 2, E=6.25, τ=0.05 ms, P=125W, t=0.6 ms. The recirculating bubble extends upstream over approximately 2 diameters, then collapses.

Efficiency

In order to assess the energetic efficiency of a "laser spike" device, it is necessary to define the overall efficiency of the system, which is different from the aerodynamic efficiency η_{ae} defined in Eq. (1). Following [35], the overall efficiency η is defined as the ratio of the fuel mass flow rate with the system to the baseline fuel mass flow rate. Defining the baseline fuel power as $P_0 = \dot{m}_0 h_F$, where $\dot{m}_0$ is the fuel mass flow rate and h_F is the fuel mass enthalpy, and defining the power with the system active as $P = (\dot{m}_0 - \delta\dot{m} - \dot{m}')h_F$, where $\delta\dot{m}$ represents the fuel savings induced by the mean drag reduction and $\dot{m}'$ is the fuel mass flow rate required to power the laser spike system. With this definition, the overall efficiency η of the system is given by

$$\eta = 1 - \langle \Delta \rangle + \varepsilon \frac{\eta_{pe}}{\eta_p} \tag{9}$$

Here, $\eta_{pe} = (DU_\infty)/(\dot{m}_0 h_F)$ is the propulsive efficiency of the body engine and $\eta_p = E/(\tau \dot{m}' h_F)$ is the efficiency of the laser spike system, converting the energy stored in the fuel into an actual energy deposited in the flow. This latter figure of merit includes the efficiency of the physical devices (such as the laser, the power conversion unit), and the efficiency of the physical processes (e.g., plasma induced heating of the gas). For the following analysis, $H = \eta_{pe}/\eta_p$, the figure of merit of the laser spike device. Having a large H means that the energy conversion is inefficient compared to the engine propulsive efficiency. At best, the value of H is around unity, although values in the range of 10-100 are more credible. Finally, the small parameter ε quantifies the ratio of the mean power deposited in the flow to the work of the drag force:

$$\varepsilon = \frac{E/\tau}{\frac{1}{2}\rho_\infty U_\infty^3 S C_X^0} \tag{10}$$

In order to analyze the efficiency of the drag reduction system, the two deposition regimes are considered. The first regime corresponds

Regime	Pulse Energy (mJ)	Repetition Period τ (ms)	Mean Power (W)	Mean drag reduction (Δ)	Efficency η		
					$H=1$	$H=10$	$H=100$
I	6.25	0.3	20	9.5%	0.90	0.91	0.97
II	6.25	0.1	62.5	19%	0.81	0.83	1.02
I	25	0.325	77	13.8%	0.86	0.89	1.12
II	25	0.2	125	20ù	0.80	0.84	1.22
I	100	0.4	250	14.3%	0.86	0.94	1.69

Table 5 - Efficiency of the repetitive pulsed energy deposition

to a deposition period τ equal to the interaction duration. The second regime takes into account the cumulative effect, for the two quasi-steady states previously identified. The results are given in Table 5 below, for three hypotheses for the laser spike efficiency ($H=1$, 10 and 100).

It appears first that the deposition in Regime II, where a cumulative effect is achieved, is more efficient in all cases in terms of drag reduction. In addition, in the first regime the next deposition occurs at the end of the interaction period of the previous energy release. This induces large drag fluctuations that are prejudicial from a technical point of view. Finally, in the case with $H=1$, corresponding to an efficient power conversion, the laser spike system is always efficient ($\eta<1$). Typically, the propulsive efficiency is within the range of 0.5-0.8. In the more realistic cases ($H\geq10$), the system is efficient as long as the laser system efficiency is not too low.

Conclusions

This study focused on the modeling of a long linear energy deposition in front of a supersonic blunt body at M=3. This figures the effect of a "virtual spike", possibly obtained by the use of femtosecond laser filaments. Single and repetitive energy depositions have been studied, considering the air plasma created as a gas at Local Thermodynamic Equilibrium. The study for a single pulse has shown that a transient drag reduction is obtained when the heated core resulting from the energy deposition interacts with the bow shock. This interaction induces a large recirculating bubble, correlated with a drop in the front pressure. This bubble evolves towards a toroidal vortex with a low pressure core, which is then convected downstream by the flow. The intensity of the drag reduction depends nonlinearly on the total energy deposition and the deposition length, while it is roughly independent of the deposition duration and its radius, within the range tested in this study. For the repetitive case, it is shown that depending on the repetition frequency, the deposition may result in the formation of a large recirculating bubble, undergoing regular collapses, or in a smaller quasi-steady recirculating bubble. This behavior is similar to what is observed for a spiked blunt body. In this case, the "length" of the spike is controlled by the mean power and repetition rate. An efficiency analysis shows that the laser spike lowers the fuel consumption by 15-20%, as long as the energy coupling efficiency of the laser system is equal to, or above, 10% of the engine propulsive efficiency ■

Acknowledgements

This study was funded by the French DGA, under the "REI, Recherche Exploratoire et Innovation" program.

References

[1] L. N. CATTAFESTA, M. SHEPLAK - *Actuators for Active Flow Control.* Annu. Rev. Fluid Mech., vol. 43, no. 1, pp. 247–272, Jan. 2011.

[2] E. MOREAU - *Airflow Control by Non-Thermal Plasma Actuators*. J. Phys. D. Appl. Phys., vol. 40, no. 3, pp. 605–636, Feb. 2007.

[3] S. B. LEONOV, J. LI, S. FU - *Review of Plasma-Based Methods for High-Speed Flow Control*. vol. 498, no. 1, pp. 498–502, 2011.

[4] L. WANG, Z. LUO, Z. XIA, B. LIU, X. DENG - *Review of Actuators for High Speed Active Flow Control*. Sci. China Technol. Sci., vol. 55, no. 8, pp. 2225–2240, May 2012.

[5] D. KNIGHT, G. ELLIOTT, G. CANDLER, A. ZHELTOVODOV - *Localized Flow Control in High Speed flows using laser energy deposition*. CCD 2003-25, 2003.

[6] R. G. ADELGREN, H. YAN, G. ELLIOT, and Al. - *Control of Edney IV Interaction by Pulsed Laser Energy Deposition*. AIAA J., vol. 43, no. 2, pp. 256–269, 2005.

[7] P. K. TRET'YAKOV, A. F. GARANIN, G. N. GRACHEV, V. L. KRAINEV, A. G. PONOMARENKO, V. N. TISHCHENKO, V. I. YAKOVLEV, G. G. CHERNYI - *Control of Supersonic Flow around Bodies by Means of High-Power Recurrent Optical Breakdown*. Phys. - Dokl., vol. 41, pp. 566–567, Nov. 1996.

[8] J.-H. KIM, A. MATSUDA, T. SAKAI, A. SASOH - *Wave Drag Reduction with Acting Spike Induced by Laser-Pulse Energy Depositions*. AIAA J., vol. 49, no. 9, pp. 2076–2078, Sep. 2011.

[9] T. SAKAI, Y. SEKIYA, M. ROSLI, A. MATSUDA, A. SASOH - *Unsteady Interaction of Blunt Bodies With Laser Induced Plasma in A Supersonic Flow*. 39th Plasmadynamics and Lasers Conference, 2008, no. AIAA 2008–3794.

[10] A. IWAKAWA, N. HASEGAWA, T. OSUKA, R. MAJIMA, T. SAKAI, A. SASOH - *Supersonic Drag Reduction Performance of Blunt-Body with Conical Spike using Energy Depositions*. 44th AIAA Plasmadynamics and Lasers Conference, 2013.

[11] A. SASOH, Y. SEKIYA, T. SAKAI, J.-H. KIM, A. MATSUDA - *Supersonic Drag Reduction with Repetitive Laser Pulses Through a Blunt Body.* AIAA J., vol. 48, no. 12, pp. 2811–2817, Dec. 2010.

[12] A. COUAIRON - *Femtosecond Filamentation in Air.* Springer series in Chemical Phisics, vol. 84, pp. 235–258, 2006.

[13] A. COUAIRON, A. MYSYROWICZ - *Femtosecond Filamentation in Transparent Media.* Phys. Rep., vol. 441, no. 2–4, pp. 47–189, 2007.

[14] A. HOUARD, Y. LIU, A MYSYROWICZ - *Recent Developments in Femtosecond Filamentation.* J. Phys. Conf. Ser., vol. 497, p. 012001, Apr. 2014.

[15] B. ZHOU, S. AKTURK, B. PRADE, Y.-B. ANDRÉ, A. HOUARD, Y. LIU, M. FRANCO, C. D'AMICO, E. SALMON, Z.-Q. HAO, N. LASCOUX, A. MYSYROWICZ - *Revival of Femtosecond Laser Plasma Filaments in Air by a Nanosecond Laser.* Opt. Express, vol. 17, no. 14, pp. 11450–11456, 2009.

[16] J. B. MICHAEL, A. DOGARIU, M. N. SHNEIDER, R. B. MILES - *Subcritical Microwave Coupling to Femtosecond and Picosecond Laser Ionization for Localized, Multipoint Ignition of Methane/air Mixtures.* J. Appl. Phys., vol. 108, no. 9, p. 93308, 2010.

[17] K. KREMEYER, K. SEBASTIAN, C.-W. SHU - *Computational Study of Shock Mitigation and Drag Reduction by Pulsed Energy Lines.* AIAA J., vol. 44, no. 8, pp. 1720–1731, 2006.

[18] G. W. SUTTON - *Effect of Laser-Induced Upstream Cylindrical Blast Waves on a High-Velocity Rocket.* AIAA J., vol. 47, no. 5, 2009.

[19] C. GREY MORGAN - *Laser-Induced Breakdown of Gases*. Rep. Prog. Phys., vol. 38, pp. 621–665, 1975.

[20] N. KROLL, K. M. WATSON - *Theoretical Study of Ionization of Air by Intense Laser Pulses.* Phys. Rev. A, vol. 5, no. 4, 1972.

[21] M. H. NIEMZ - *Threshold Dependence of Laser-Induced Optical Breakdown on Pulse Duration.* Appl. Phys. Lett., vol. 66, no. 10, p. 1181, 1995.

[22] R. KANDALA, G. CANDLER - *Numerical Studies of Laser-Induced Energy Deposition for Supersonic Flow Control.* AIAA J., vol. 42, no. 11, 2004.

[23] A. D'ANGOLA, G. COLONNA, C. GORSE, M. CAPITELLI - *Thermodynamic and Transport Properties in Equilibrium Air Plasmas in a Wide Pressure and Temperature Range*. Eur. Phys. J. D, vol. 46, no. 10, 2008.

[24] A. REFLOCH, B. COURBET, A. MURRONE, P. VILLEDIEU, C. LAURENT - *CEDRE Software.* Aerosp. Lab J., no. 2, pp. 1–10, 2011.

[25] P. CHEVALIER, B. COURBET, D. DUTOYA, P. KLOTZ, E. RUIZ, J. TROYES, P. VILLEDIEU - *CEDRE : Development and Validation of a Multiphysics Computational Software.* 1st european conference for aerospace science (EUCASS), 2005.

[26] D. DUTOYA, L. MATUSZEWSKI - *Thermodynamics in CEDRE.* Aerosp. Lab J., no. 2, pp. 1–11, 2011.

[27] R. CÉRÉSUELA - *Maquettes étalons HB.1 et HB.2. Caractéristiques aérodynamiques mesurées dans les souffleries de l'ONERA de Mach 2 à Mach 16.5.* ONERA-NT 123, 1968.

[28] R. CÉRÉSUELA - *Mesure d'efforts et de pression sur la maquette balistique étalon HB2.* ONERA-NT 13/1879A 1964.

[29] A. AMBROSIO, A. WORTMAN - *Stagnation Point Shock Detachment Distance for Flow around Spheres and Cylinders*. ARS J., vol. 32, p. 281, 1962.

[30] V. M. FOMIN, A. A. MASLOV, N. D. MALMUTH, V. P. FOMICHEV, A. P. SHASHKIN, T. A. KOROTAVA, A. N. SHIPLYUK, G. A. POZDNYAKOV - *Influence of Counterflow Plasma Jet on Supersonic Blunt-Body Pressures.* AIAA J., vol. 40, no. 6, pp. 1170–1177, 2002.

[31] M. GOLBABAEI-ASL, D. D. KNIGHT - *Numerical Characterization of High-Temperature Filament Interaction with Blunt Cylinder at Mach 3.* Shock Waves, vol. 24, no. 2, pp. 123–138, Aug. 2013.

[32] A.G. PANARAS - *Pulsating Flow about Axisymmetric Concave Bodies.* AIAA J., vol. 19, no. 6, pp. 804–806, 1981.

[33] P.-Q. ELIAS - *Effets de plasmas sur une onde de choc supersonique à Mach 3.* Thèse de doctorat en Energétique de l'Ecole Centrale Paris, 2007.

[34] J. SRULIJES, P. GNEMMI, K. RUNNE, F. SEILER - *High-Pressure Shock Tunnel Experiments and CFD Calculations on Spike-Tipped Blunt Bodies.* 22nd AIAA Aerodynamic Measurement Technology and Ground Testing Conference, 2002.

[35] P.-Q. ELIAS, B. CHANETZ, S. LARIGALDIE, D. PACKAN - *Study of the Effect of Glow Discharges Near a M 3 Bow Shock.* AIAA J., vol. 45, no. 9, pp. 2237–2245, 2007.

Acronyms

CFD	(Computational Fluid Dynamics)
LTE	(Local Thermodynamic Equilibrium)
URANS	(Unsteady Reynolds-Averaged Navier-Stokes)

AUTHOR

Paul-Quentin Elias is a Research Scientist at ONERA, in the Lightning & Plasma Applications Group. He holds an Engineering degree and a PhD from Ecole Centrale Paris. His main interests are the applications of cold or thermal plasmas to aerospace systems. His current activities involve the development of optical diagnostics for lightning and atmospheric pressure discharges, the development and characterization of plasma actuators for flow control applications and the testing and modeling of new low pressure plasma sources for electric propulsion. Paul-Quentin Elias has authored or co-authored 12 peer-reviewed articles, 3 invited conferences and more than 40 technical reports.